Ceramics International 47 (2021) 9068–9074

Contents lists available at ScienceDirect

Ceramics International

journal homepage: www.elsevier.com/locate/ceramint

The $Sr_{2.4}Dy_{0.6}Co_2O_{7-\delta}$ Ruddlesden–Popper Phase: Structural, thermoelectric, and magnetic properties

V.A. Dudnikov [a], Yu S. Orlov [a,b,*], L.A. Solovyov [c], S.N. Vereshchagin [c], S. Yu Gavrilkin [d]

[a] Kirensky Institute of Physics, Krasnoyarsk Scientific Center, Siberian Branch, Russian Academy of Sciences, Krasnoyarsk, 660036, Russia
[b] Siberian Federal University, Krasnoyarsk, 660041, Russia
[c] Institute of Chemistry and Chemical Technology, Krasnoyarsk Scientific Center, Siberian Branch, Russian Academy of Sciences, Krasnoyarsk, 660036, Russia
[d] Lebedev Physical Institute, Russian Academy of Sciences, Moscow, 119991, Russia

ARTICLE INFO

Keywords:
Rare-earth substituted cobalt oxides
Ruddlesden–Popper phase
Thermoelectric oxide materials
Magnetic properties

ABSTRACT

–A new anion-deficient $Sr_{2.4}Dy_{0.6}Co_2O_{7-\delta}$ (δ = 0.33–1.1) perovskite phase with a structure of the $A_3B_2O_7$ Raddlesden–Popper homologous series has been obtained by the solid-state synthesis in the reducing/oxidizing atmosphere and its structural characterization has been performed by the Rietveld refinement of the X-ray powder diffraction data. It has been stablished that the $Sr_{2.4}Dy_{0.6}Co_2O_{7-\delta}$ compound (sp. gr. *I4/mmm*) has parameters of $a = b = 3.8526(1)$ and $c = 19.9431(7)$ Å in the reduced form ($\delta = 1.1$) and $a = b = 3.8086(1)$ and $c = 19.9190(6)$ Å in the oxidized form ($\delta \approx 0.33$) and oxygen vacancies occupy mainly the sites linking CoO_5 polyhedra inside two perovskite layers. It has been established using differential scanning calorimetry and thermogravimetry that, at $T < 530$ K, the synthesized phase is stable against the inert and oxidizing atmosphere; at higher temperatures, the $Sr_{2.4}Dy_{0.6}Co_2O_{7-\delta}$ compound can reversibly absorb/release oxygen. The magnetic properties of the $Sr_{2.4}Dy_{0.6}Co_2O_{6.09}$ compound have been investigated in the temperature range of 10–400 K and described in terms of the formation of dimers, in which the Co^{3+}–Co^{3+} and Co^{2+}–Co^{2+} ion pairs antiferromagnetically interact and are in the nonmagnetic ground state. The electrical conductivity and the Seebeck coefficient have been measured in air in the temperature range from 300 to 800 K. An observed sharp decrease in the Seebeck coefficient of the $Sr_{2.4}Dy_{0.6}Co_2O_{7-\delta}$ compound and the change in its sign near 700 K have been attributed to the transition of cobalt ions to the Co^{3+} state and the charge disproportionation of Co^{3+} ions to Co^{2+} and Co^{4+} ones.

1. Introduction

Over the last few decades, the compounds with a perovskite and perovskite-like structure based on complex transition metal oxides, their amazing properties, and a high potential for application as functional materials have attracted close attention of researches. The Raddlesden–Popper (RP) phases with general formulas $AO(ABO_3)_n$ or $A_{n+1}B_nO_{3n+1}$ (A is a rare-earth or alkaline-earth metal and B is a transition metal) were first investigated in titanates [1,2]. These phases have a tetragonal structure consisting of intergrown ABO_3 perovskite layers and AO rock salt structure fragments in the sequence $–(ABO_3)_n–(AO)–(ABO_3)_n–(AO)–$. The shift of ABO_3 perovskite blocks relative to each other by 1/2 of the perovskite subcell diagonal of the (001) plane along the *c* axis leads to the layered structure. The integer *n* is the number of perovskite layers coupled by means of vortex-sharing octahedra [3], which is consistent with the number of a term in the homological series. The limiting case $n = \infty$ corresponds to the perovskite-type structure. The physical properties of such phases depend mainly on the valence state of ions, the number of perovskite layers *n*, and the oxygen content. Moreover, the oxygen contents in each specific compound can be significantly different [4] and, in some compounds, either much lower or higher than the normal value [5]. Similar to the classical compounds with a perovskite structure, the RP phases can exhibit superconductivity [6,7], colossal magnetoresistance [8], ferromagnetism [4,9] antiferromagnetism [10] and catalytic activity [11]. The thorough investigations of these systems showed that they are promising for use as solid oxide fuel cells [12–18], thermoelectrics [19,20], and capacitor materials [21].

The RP phases, similar to the ABO_3 perovskites [22,23] with cobalt ions acting as transition metal ions, have a feature caused by the

* Corresponding author. Kirensky Institute of Physics KSC SB RAS, Krasnoyarsk, 660036, Russia; ,
E-mail addresses: jso.krasn@mail.ru, orlov@iph.krasn.ru (Y.S. Orlov).

https://doi.org/10.1016/j.ceramint.2020.12.030
Received 5 August 2020; Received in revised form 1 December 2020; Accepted 4 December 2020
Available online 5 December 2020
0272-8842/© 2020 Elsevier Ltd and Techna Group S.r.l. All rights reserved.

competition of different spin states of the Co^{3+} ion. The proximity of the crystalline field and Hund exchange energy can violate the Hund's rule and, instead of the high-spin (HS) ground state with the spin S = 2, the low-spin (LS) term with S = 0 for the d^6 shell electron of Co^{3+} ionsis stable. This determines the specific electronic, magnetic, and thermodynamic properties of the RP phases. Therefore, in addition to the different Co^{2+}, Co^{3+}, and Co^{4+}oxidation states, different possible spin states (LS (S = 0), IS (S = 1), and HS (S = 2)) and coordination (pyramidal, octahedral, and tetrahedral) cobalt environment multiplicity fluctuations can occur, which broadens even more the range of physical properties.

In contrast to a wide series of $Ln_{2-x}Sr_xCoO_4$ cobaltites with an RP structure with $n = 1$, single-phase RP samples with $n = 2$ (A, A′)$_{n+1}B_2O_{7-\delta}$ with heterovalent substitution in the A site and Co in the B site are formed quite rarely [4,9,24,25]. The lack of data on these compounds is apparently caused by the frequent occurrence of additional phases during the synthesis.

In this study, we present the data on the synthesis of a new single-phase $Sr_{2.4}Dy_{0.6}Co_2O_{7-\delta}$ compound with a structure of the second term of the $A_3B_2O_7$ RP homologous series and examine its structural, magnetic, and thermoelectric properties.

2. Experimental

Polycrystalline $Sr_{2.4}Dy_{0.6}Co_2O_{7-\delta}$ samples were synthesized by a standard ceramic technology. A well-homogenized mixture of stoichiometric amounts of high-purity Co_3O_4 (99.7%, metals basis) and Dy_2O_3 (99.99%, REO) oxides and $SrCO_3$ (99.99%, metals basis) carbonate was annealed at 1473 K for 24 h with intermediate grinding and subsequent pressing in disk-shaped tablets with a diameter of 20 mm and a thickness of 2 mm. The disks were annealed at 1473 K for 8 h and cooled to room temperature at a rate of 2 K/min. Then, bar-shaped samples 5 × 13 × 2 mm in size were cut from the synthesized disks. The bars were annealed in pure helium (99.999 vol% of He) at 1458 K for 3 h, cooled down to 1073 K at a rate of 2 K/min and to 723 K at a rate of 10 K/min, and then reduced at this temperature in the 5% H_2–He mixture for 3 h. After that, the samples were cooled to room temperature at a rate of 2 K/min in the 5% H_2–He flow, flushed with helium, and stored without precautions under ambient condition. The $Sr_{2.4}Dy_{0.6}Co_2O_{7-\delta}$ sample synthesized using this procedure is hereafter referred to as SDC-RP2-red. The "oxidized" sample prepared by annealing of sample SDC-RP2-red in air at 800 K for 2 h is referred to as SDC-RP2-ox.

The X-ray powder diffraction (XRPD) data were collected using a PANalyticalX'Pert PRO diffractometer equipped with a PIXcel solid state detector (CoKα radiation) over the 2θ angle range of 6–158°. Powder samples were prepared by grinding with octane in an agate mortar and packed into a flat sample holder for the XRPD measurements in the Bragg–Brentano geometry. The full-profile crystal structure refinement was performed using the derivative difference minimization (DDM) method [26].

The oxygen content was determined with a TG-DSC NETZSCH STA 449C analyzer from the mass loss Δm(%) [27] when the grinded sample with a particle size of smaller than 50 μm are reduced in the 5% H_2-Ar flow upon heating to 1173 K at a rate of 15 K/min assuming that cobalt is reduced to the metallic state. The reduction occurred in an open corundum crucible; the sample mass was 20 ± 0.5 mg. The measurements were performed with the buoyancy force correction; i.e., the control measurement data for an empty crucible (zero line) were obtained under the same conditions. The oxygen nonstoichiometry index determination error was δ = ± 0.01.

The simultaneous thermal analysis (STA) experiments were conducted on a TG-DSC NETZSCH STA 449C analyzer equipped with an Aeolos QMS 403C mass spectrometer. The ceramic bar used in the resistivity measurements was crushed and a piece of 15 ± 0.5 mg (about 3 × 1 × 1 mm in size) was subjected to the thermal analysis. The differential scanning calorimetry (DSC) and thermogravimetry (TG) investigations were carried out in platinum crucibles with perforated lids in the dynamic 20% O_2–Ar or pure (99.999%) Ar atmosphere under ambient pressure.

The temperature and field dependences of the magnetization were measured in the temperature range from 10 to 400 K in fields of up to 9 T on a Quantum Design Physical Property Measurement System (PPMS-9) (US) at the Lebedev Physical Institute of the Russian Academy of Sciences (Moscow).

The temperature dependences of the Seebeck coefficient and electrical resistivity were obtained on an experimental setup for the thermopower and resistivity measurements similar to that described in [28] at the Kirensky Institute of Physics, Siberian Branch of the Russian Academy of Sciences (Krasnoyarsk).

3. Results and discussion

3.1. $Sr_{2.4}Dy_{0.6}Co_2O_{7-\delta}$ structure

According to the XRD data, sample SDC-RP2-red represents a perovskite-like phase, which belongs to the $AO(ABO_3)_n$ RP homologous series ($n = 2$). The structure reflects the intergrown double perovskite (ABO_3) and single rock salt (AO) layers and should correspond to the stoichiometric $A_3B_2O_7$ composition.

Fig. 1 shows the observed, calculated, and difference XRPD profiles after the DDM refinement for sample SDC-RP2-red at 298 K; the crystallographic data are given in Table 1. Sample SDC-RP2-ox has a similar structure. The crystallographic parameters are also given in Table 1. The profile is fitted almost perfectly up to the highest 2θ values, which is indicative of the high quality of the refinement. A tetragonal superstructure (symmetry sp. gr. $I4/mmm$) was established.

The XRD data show that the synthesized RP phase is highly nonstoichiometric (see the structure in Fig. 2). There are two independent A sites occupied by Sr^{2+} or Sr^{2+}/Dy^{3+} ions, one Co type, and three independent oxygen ions. The structure consists of the ordered double layers of CoO_5 corner pyramids intergrown with the SrO rock salt-type layers. Sr^{2+}/Dy^{3+} ions are ordered in the alternating layers along the c axis. Inside the double pyramidal cobalt layers, Sr^{2+} and Dy^{3+} cations are statistically distributed and oxygen vacancies are mainly located in the sites linking the CoO_5 polyhedra inside two perovskite layers (the O1 site). This structure qualitatively corresponds to the structure of cobaltites $Sr_3Co_2O_{6.13}$ [29] and $Sr_2Y_{0.8}Ca_{0.2}Co_2O_6$ [10], manganites $Sr_3Mn_2O_{6+x}$ [30], and cuprates $La_2SrCu_2O_6$ [31].

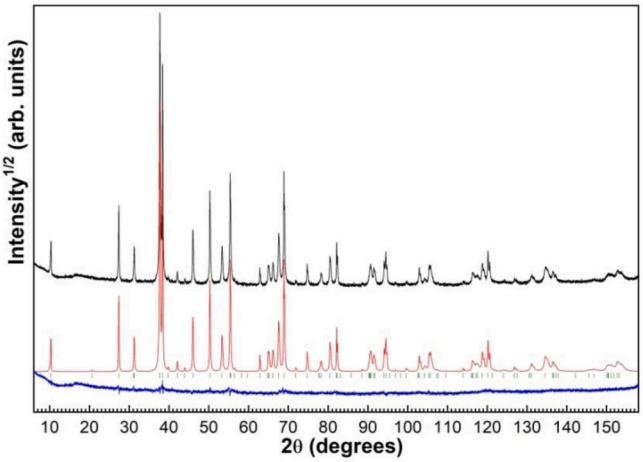

Fig. 1. Observed (black, on the top), calculated (red, in the middle), and difference (blue, in the bottom) XRPD profiles after the DDM refinement of the $Sr_{2.4}Dy_{0.6}Co_2O_{7-\delta}$ crystal structure at 298 K. The calculated peak positions are marked. (For interpretation of the references to colour in this figure legend, the reader is referred to the Web version of this article.)

Table 1
Crystal lattice (tetragonal *I4/mmm*) parameters, atomic coordinates, site occupancies, and isotropic displacement factors for the $Dy_{0.6}Sr_{2.4}Co_2O_{7-\delta}$ compound.

Structural formula: $Dy_{0.58}Sr_{2.42}Co_2O_{5.82}$						
Lattice parameters: $a = b = 3.8526(1)$ and $c = 19.9431(7)$ Å						
Rfactors: $R_{Bragg} = 2.9\%$ and $R_{DDM} = 4.3\%$						
Atom	Site	Occ.	x	Y	z	Uiso, Å^2
Sr1	2b	0.422(18)	0	0	1/2	0.025(3)
Dy1	2b	0.578(18)	0	0	1/2	0.025[a]
Sr2	4e	1	1/2	1/2	0.18168(8)	0.022(3)
Co	4e	1	0	0	0.09862(16)	0.020(4)
O1	2a	0.14(3)	0	0	0	0.063[a]
O2	4e	1	0	0	0.19602(48)	0.028(6)
O3	8 g	0.921(15)	0	1/2	0.07640(31)	0.041(6)
Structural formula: $Dy_{0.58}Sr_{2.42}Co_2O_{6.64}$						
Lattice parameters: $a = b = 3.8086(1)$ and $c = 19.9190(6)$ Å						
Rfactors: $R_{Bragg} = 2.0\%$ and $R_{DDM} = 4.0\%$						
Atom	Site	Occ.	x	Y	z	Uiso, Å^2
Sr1	2*b*	0.423(9)	0	0	1/2	0.035(2)
Dy1	2*b*	0.577(9)	0	0	1/2	0.035[a]
Sr2	4*e*	1	1/2	1/2	0.18154(4)	0.020(2)
Co	4*e*	1	0	0	0.09757(8)	0.017(2)
O1	2*a*	0.639(15)	0	0	0	0.063(12)
O2	4*e*	1	0	0	0.19308(22)	0.026(4)
O3	8*g*	1	0	1/2	0.08628(21)	0.038(4)

[a] These parameters were constrained.

Below, for brevity, the subscripts in the chemical formulae of the investigated samples are rounded off to the nearest tenth.

3.2. TG-DSC thermal stability data for the $Sr_{2.4}Dy_{0.6}Co_2O_{7-\delta}$ compound

3.2.1. Thermal stability of the $Sr_{2.4}Dy_{0.6}Co_2O_{7-\delta}$ compound in a reducing atmosphere

Fig. 3a (curve *1*) shows a TG curve corresponding to the reduction of sample SDC-RP2-red in the 5% H_2–Ar flow. A total mass loss was found to be $\Delta m = -7.99\%$ (40–1200 K); reaction (1); therefore, the stoichiometry of the initial RP phase is $Sr_{2.4}Dy_{0.6}Co_2O_{5.9}$. The oxygen content determined from the direct reduction of sample SDC-RP2-red is inconsistent with that obtained by the DDM refinement (Table 2). The oxygen content discrepancy between the refined structural formulae can be attributed to the well-known deviations of the ionic scattering curves from the real electron distribution in the crystals.

It can be seen in Fig. 3a that the $Sr_{2.4}Dy_{0.6}Co_2O_{5.9}$ RP phase is relatively stable at $T < 690$ K. The subsequent reduction occurs in two stages (Table 2), which appear as pronounced water evolution peaks (curve *3* in Fig. 3a) with the corresponding effects in the TG curve and exo effects in the DSC curve. A deeper reduction is observed at 690–860 K and an extended plateau at 820–980 K between stages I and II points out the formation of undetermined stable products (phases).

$$Sr_{2.4}Dy_{0.6}Co_2O_{5.90} + 1.3H_2 = 2.4\ SrO + 0.3\ Dy_2O_3 + 2\ Co + 2.6H_2O,\ \Delta m = -7.99\% \quad (1)$$

$$Sr_{2.4}Dy_{0.6}Co_2O_{z1} \Leftrightarrow Sr_{2.4}Dy_{0.6}Co_2O_{z2} + (z1 - z2)/2\ O_2 \quad (2)$$

T_m is the temperature of the maximum water evolution rate.

3.2.2. Thermal stability of the $Sr_{2.4}Dy_{0.6}Co_2O_{7-\delta}$ compound in a nonreducing atmosphere

The synthesized $Sr_{2.4}Dy_{0.6}Co_2O_{5.90}$ phase SDC-RP2-red is stable under the nonoxidizing condition. Only a minor mass variation ($\Delta m = 0.05\%$) was observed upon heating the sample from 40 to 1000 K in pure (99.999%) Ar (curve *1* in Fig. 3b).

Upon heating the $Sr_{2.4}Dy_{0.6}Co_2O_{5.90}$ sample to 550–570 K under the oxidizing conditions (20% O_2–Ar), no mass variation occurred (onset of curve *2* in Fig. 3b). Further heating to 747 K led to the mass growth, which indicated oxidation of cobalt, and a progressive decline at $T >$ 747 K. When the sample is slowly (at a rate of ~2 K/min) cooled from

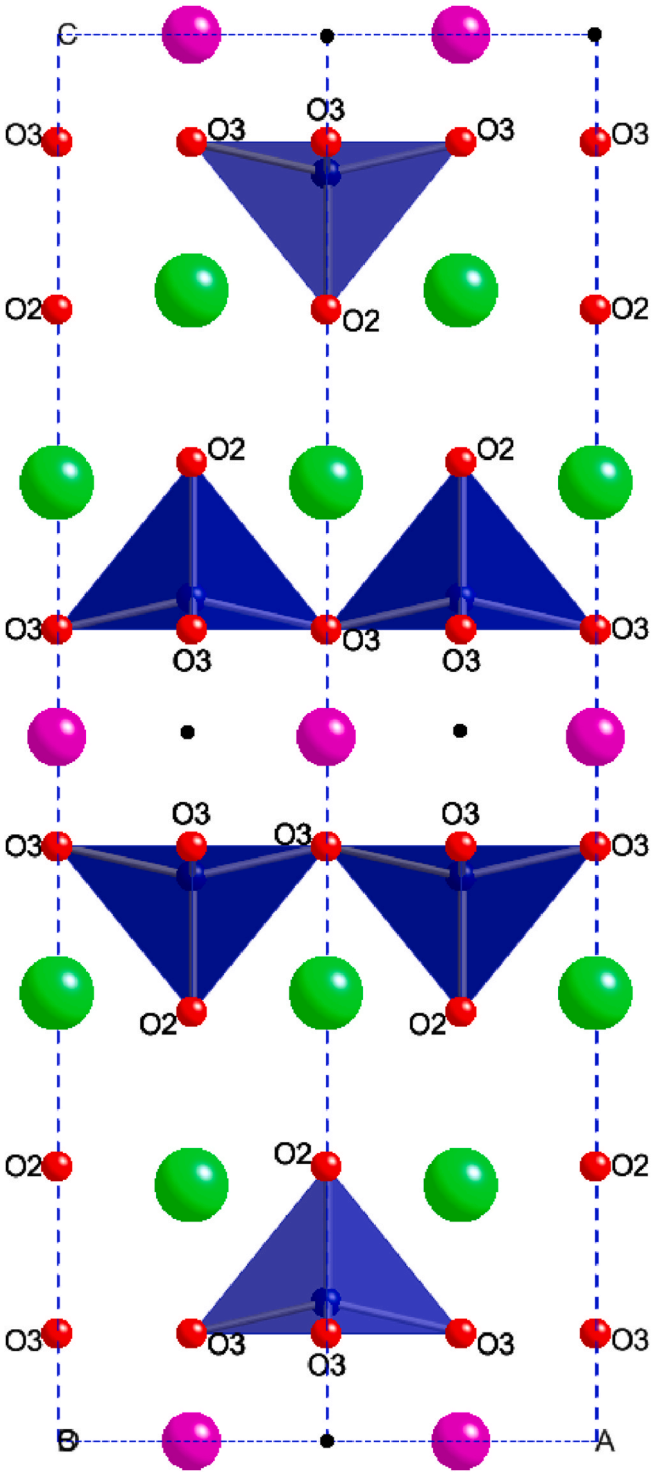

Fig. 2. Perfect $Sr_{2.4}Dy_{0.6}Co_2O_6$ structure (green – Sr, purple – Dy/Sr, red – oxygen (O2 and O3 sites), and blue –square pyramids corresponding to the cobalt environment). Small black points show the O1 site (location of oxygen vacancies). (For interpretation of the references to colour in this figure legend, the reader is referred to the Web version of this article.)

1273 to 298 K in air or in the 20% O_2–Ar flow, it absorbs oxygen with the formation of the SDC-RP2-ox phase with the $Sr_{2.4}Dy_{0.6}Co_2O_{6.67}$ composition, which was determined from H_2 reduction (curve *2* in Fig. 3a). This "oxidized" phase belongs to the same tetragonal *I4/mmm* symmetry with partially filled O1 oxygen sites (Table 1). The $Sr_{2.4}Dy_{0.6}Co_2O_{6.67}$ compound is stable against the oxidizing (20%

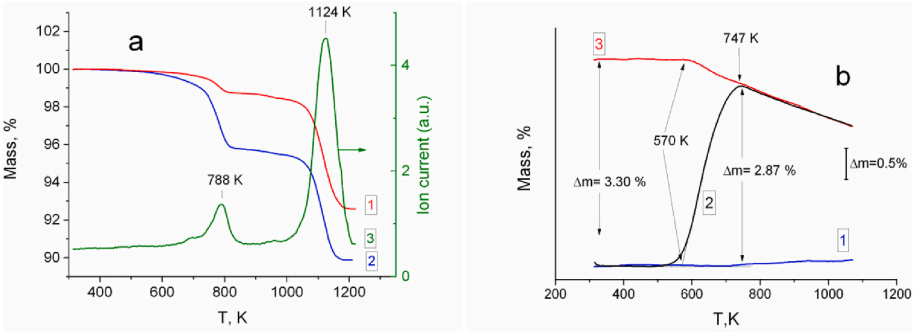

Fig. 3. (a) Thermogravimetry data on (*1*, red) reduced sample SDC-RP2-red and (*2*, blue) oxidized sample SDC2-RP2-ox collected in the 5% H_2–Ar flow in the range from 313 to 1200 K (β = 15 K/min). Curve *3* (mass-spectral intensity of the H_2O + ion, *m*/z = 18, olive) illustrates the formation of water upon reduction of sample SDC2-RP2-ox. (b) Variation in the $Sr_{2.4}Dy_{0.6}Co_2O_{7-\delta}$ sample mass with temperature and gas phase composition, β = 10 K/min (*1*, blue) SDC-RP2-red, Ar; (*2*, black) SDC-RP2-red, 20% O_2–Ar; and (*3*, red) SDC-RP2-ox, 20% O_2–Ar. (For interpretation of the references to colour in this figure legend, the reader is referred to the Web version of this article.)

Table 2
Thermal effects for reduction (5% H_2–Ar, β = 10 K/min) of sample SDC-RP2-red.

Stage	Temperature of the effect, K	T_m, K	Δ*m*, %	Δ*H*
I	(690)–860	788	–1.84	Exo
II	900–1200	1124	–6.15	Exo

O_2–Ar) atmosphere up to ~570 K and, above this temperature, starts losing oxygen (curve *3* in Fig. 3b).

The repeated $Sr_{2.4}Dy_{0.6}Co_2O_{7-\delta}$ heating–cooling cycles in the oxidizing (20% O_2–Ar), inert (99.999% Ar), or reducing (5% H_2–Ar, $T <$ 723 K) atmosphere are accompanied by the reproducible smooth mass variation, according to the TG data (Fig. 3b). The XRPD data and the absence of pronounced DSC thermal effects suggest that the observed behavior results from the change in the RP-phase nonstoichiometry (reaction (2)), rather than from some chemical or structural phase transformations.

Thus, the thermal analysis data showed that the composition of both the "reduced" $Sr_{2.4}Dy_{0.6}Co_2O_{5.90}$ and "oxidized" $Sr_{2.4}Dy_{0.6}Co_2O_{6.67}$ RP phases is constant at $T <$ 530 K, regardless of the partial oxygen pressure. At higher temperatures, the $Sr_{2.4}Dy_{0.6}Co_2O_{7-\delta}$ compound can reversibly absorbs/release oxygen.

3.3. Magnetic properties

The magnetic properties were explored on a sample with an oxygen nonstoichiometry index of about 1. The temperature dependence of the $Sr_{2.4}Dy_{0.6}Co_2O_{5.90}$ susceptibility χ obtained in a magnetic field of 5 kOe is shown in Fig. 4a (red solid line). The plots recorded under the zero-field cooling (ZFC) and field-cooling (FC) conditions are absolutely identical. The susceptibility monotonically increases as the temperature grows. The temperature dependence of the inverse magnetic susceptibility χ^{-1} includes two portions, which are well-approximated by linear dependences corresponding to the Curie–Weiss law $\chi = C/(T - \Theta_C)$ (inset in Fig. 4a) in the low-temperature (LT) region and in the high-temperature (HT, above 200 K) region (*C* is the Curie constant and Θ_C is the asymptotic Curie temperature).

Based on the linear dependences and the formula for calculating the effective magnetic moment $\mu_{eff} = \sqrt{C \cdot 3k_B/N_A}$ (k_B is the Boltzmann constant and N_A is the Avogadro number), for the LT region we obtained $\Theta_C \approx -5$ K, $C = 8.57$ cm^3 K/mol, and μ_{eff} (LT) = 1.07μ_B and, for the HT region, $\Theta_C \sim -105$ K, $C = 14.19$ cm^3 K/mol, and μ_{eff}(HT) = 8.28μ_B. The comparison of the experimental $\chi(T)$ dependence for the $Sr_{2.4}Dy_{0.6}Co_2O_{5.90}$ sample with the $\chi_{Dy}(T)$ dependence for free Dy^{3+} ions obtained using the formula

$$\chi_{Dy} = 0.6 \cdot N_A \frac{g_J^2 \mu_B^2 J(J+1)}{3k_B(T - \Theta_{LT})} \quad (3)$$

where

$$g_J = 1 + \frac{J(J+1) + S(S+1) - L(L+1)}{2J(J+1)} = 1.33 \quad (4)$$

$J = 15/2$ (for the ground $^6H_{15/2}$ term of a free Dy^{3+} ion), $L = 5$, and $S = 5/2$ [32] showed the coincidence of these dependences in the LT region (Fig. 4a). As the temperature increases, the dependences become different and the difference between the dependences of the magnetic susceptibilities for the $Sr_{2.4}Dy_{0.6}Co_2O_{5.90}$ compound and free Dy^{3+} ions also grows (the upper red solid curve in Fig. 4a corresponds to the experimental data and the lower blue solid curve, to the theoretical dependence for Dy^{3+} ions). This can be explained by the occurrence of an additional contribution of cobalt ions.

At the oxygen deficiency δin the $Sr_{2.4}Dy_{0.6}Co_2O_{7-\delta}$ system, Co^{3+} and Co^{2+} ions coexist in a pyramidal environment (Fig. 2) and, according to

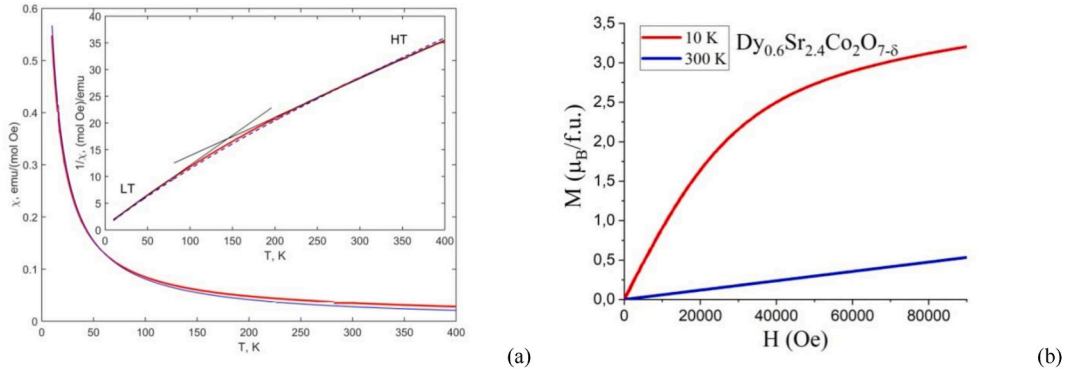

Fig. 4. (a) Temperature dependence of magnetic susceptibility for the $Sr_{2.4}Dy_{0.6}Co_2O_{5.90}$ compound in a magnetic field of H = 5 kOe (red solid line) and theoretically calculated magnetic susceptibility of Dy^{3+} ions (blue solid line). Inset: inverse susceptibility vs temperature with the Curie–Weiss approximation fitted by straights. The dashed blue line corresponds to the theoretical calculation for $Sr_{2.4}Dy_{0.6}Co_2O_{5.90}$. (b) Magnetic field dependences of magnetization for the $Sr_{2.4}Dy_{0.6}Co_2O_{5.90}$ sample at different temperatures. (For interpretation of the references to colour in this figure legend, the reader is referred to the Web version of this article.)

[33,34], are in the HS state with the spins $S_{Co^{3+}} = 2$ and $S_{Co^{2+}} = 3/2$, respectively. Since the low-temperature dependence of the magnetic susceptibility for the $Sr_{2.4}Dy_{0.6}Co_2O_{5.90}$ sample is well-described by the contribution of only Dy^{3+} ions (Fig. 4a), it can be assumed that cobalt ions form dimers, in which the Co^{3+}–Co^{3+} and Co^{2+}–Co^{2+} ionic pairs antiferromagnetically interact and are in the nonmagnetic ground state. A similar situation caused by the dimer formation is observed in the nonstoichiometric $Sm_{1-x}Ca_xCoO_{3-\delta}$ compound [35]. With an increase in temperature, the nearest magnetic states of such dimers are thermally populated, which results in the growth of the $Sr_{2.4}Dy_{0.6}Co_2O_{5.90}$ magnetic susceptibility and the deviation from χ_{Dy}. The molar magnetic susceptibility of antiferromagnetic cobalt ion dimers of two types can be presented as

$$\chi_D^a = N_a g\mu_B \frac{\sum_{S_a} S_a(S_a+1)(2S_a+1)e^{-E_a\left(J_{ex}^a, S_a\right)/k_BT}}{3k_BT\sum_{S_a}(2S_a+1)e^{-E_a/k_BT}} \quad (5)$$

where the subscripts $a = 1, 2$ indicate Co^{3+} and Co^{2+} ions, respectively; S_a is the total spin ($S_1 = 2S_{Co^{3+}}, 2S_{Co^{3+}} - 1, \ldots, 0 S_2 = 2S_{Co^{2+}}$, $2S_{Co^{2+}} - 1, \ldots, 0$), and N_a is the number of dimers per mole of $Sr_{2.4}Dy_{0.6}Co_2O_{7-\delta}$ ($N_1 \approx N_A(1.7 - \delta)$, $N_2 = N_A(\delta - 0.7)$). The energy of the a-th dimer is determined by its total spin S_a and the exchange interaction integral J_{ex}^a

$$E_a\left(J_{ex}^a, S_a\right) = -J_{ex}^a[S_a(S_a+1) - 2s_a(s_a+1)] \quad (6)$$

where $s_1 = S_{Co^{3+}}$ and $s_2 = S_{Co^{2+}}$. The total magnetic susceptibility of the $Sr_{2.4}Dy_{0.6}Co_2O_{7-\delta}$ sample can be presented as a sum of two contributions $\chi = \chi_{Dy} + \chi_D$, where $\chi_D = \chi_D^1 + \chi_D^2$. In Fig. 4a (inset), the blue dashed line corresponds to the results calculated at $J_{ex}^1 = J_{ex}^2 = -60$K and $\delta = 1.1$. Good agreement with the experimental data (the red solid line) confirms the assumptions made.

3.4. Thermoelectric properties

The electrical resistance of both the "reduced" $Sr_{2.4}Dy_{0.6}Co_2O_{5.90}$ and "oxidized" $Sr_{2.4}Dy_{0.6}Co_2O_{6.67}$ RP phases were measured in air in the temperature range of 300–800 K. The temperature dependences of resistivity ρ and conductivity σ are shown in Fig. 5a by curve *1* for $\delta = 1.1$ and curve *2* for $\delta = 0.33$. Although these dependences are qualitatively consistent with the semiconductor behavior $d\rho/dT < 0$, the courses of the curves for two samples are significantly different. The data processing in coordinates $ln\rho$ and $1/T$ (Fig. 5b) showed that, at temperatures of up to $T = 700$ K, the behavior of the resistance obeys the standard thermoactivation law

$$\rho(T) = \rho_\infty \exp(Ea/kT) \quad (7)$$

with an activation energy of $E_a = 0.28$ eV for the "reduced" $Sr_{2.4}Dy_{0.6}Co_2O_{5.90}$ phase and $E_a = 0.15$ eV for the "oxidized" $Sr_{2.4}Dy_{0.6}Co_2O6_{6.67}$ phase. Above 700 K, the electrical conductivity σ of the $Sr_{2.4}Dy_{0.6}Co_2O_{5.90}$ compound essentially grows (inset in Fig. 5a), while the electrical conductivity of the $Sr_{2.4}Dy_{0.6}Co_2O_{6.67}$ sample does not deviate from the thermoactivation law.

The temperature dependences of the Seebeck coefficient S of the samples are also noticeably different (Fig. 5c). Around room temperature, the S value for the $Sr_{2.4}Dy_{0.6}Co_2O_{5.90}$ compound is almost three times as high as that for $Sr_{2.4}Dy_{0.6}Co_2O_{6.67}$ and has a sharp minimum at $T \sim 710$ K, which passes to the range of negative values. The temperature region of the anomalous σ portion and the anomaly of the Seebeck coefficient in the temperature range of 650–730 K coincide with those for the case of $Sr_{2.4}Dy_{0.6}Co_2O_{5.90}$ oxidation revealed by the TG-DSC analysis (curve *2* in Fig. 3b). For the $Sr_{2.4}Dy_{0.6}Co_2O_{5.90}$ phase, the changes in the behavior of the electrical resistance and Seebeck coefficient with decreasing temperature are irreversible. The $Sr_{2.4}Dy_{0.6}Co_2O_{6.67}$ phase is stable against cooling/heating in air and exhibits no anomalies in the temperature dependences of the electrical conductivity σ and the Seebeck coefficient S (Fig. 5a and c).

A positive Seebeck coefficient (Fig. 5c) indicates that the majority

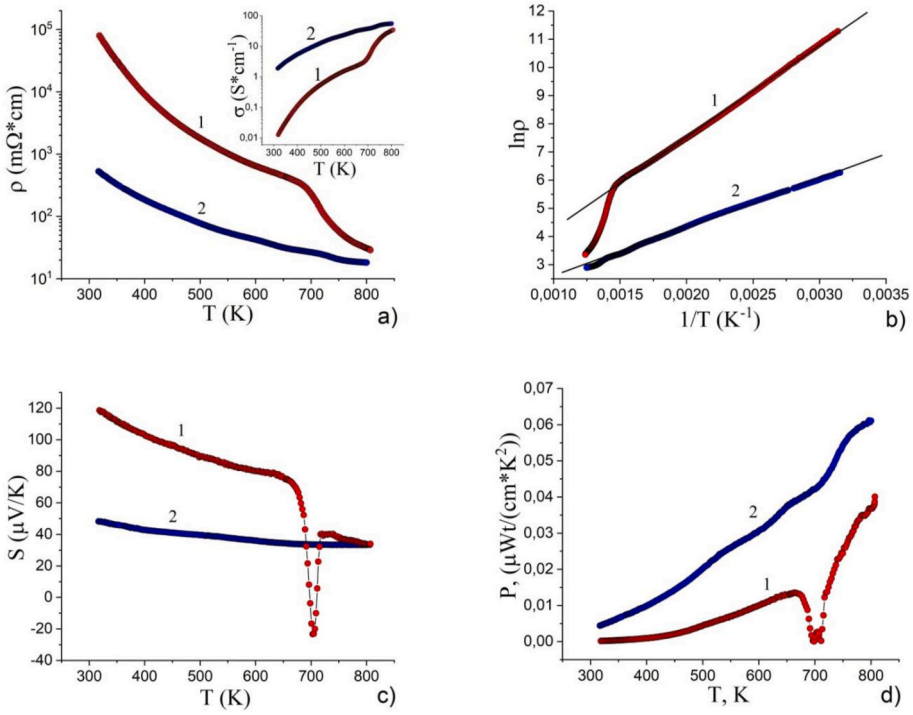

Fig. 5. (a) Temperature dependences of resistivity ρ and conductivity σ (insert), (b) ln(ρ) versus $1/T$ plots, (c) Seebeck coefficient S, and (d) thermoelectric power factor P versus temperature T for the $Sr_{2.4}Dy_{0.6}Co_2O_{7-\delta}$ phase at $\delta = 1.1$ (curves *1*) and $\delta = 0.33$ (curves *2*). Straight lines (b) show the correspondence to the activation law.

carriers are holes in the temperature ranges of $T < 690$ K and $T > 720$ K; a negative S value points out the dominance of electron conductivity at temperatures from 690 to 720 K.

At the stoichiometry change from $Sr_{2.4}Dy_{0.6}Co_2O_{5.82}$ to $Sr_{2.4}Dy_{0.6}Co_2O_{6.64}$ ("reduced" and "oxidized"), no structural transitions were detected, which is proved by the XRPD profiles after the DDM refinement (Table 1) and consistent with the absence of effects related to structural transitionsin the thermal analysis data. Therefore, we can conclude that the observed temperature anomaly of the Seebeck coefficient is not caused by a structural phase transition.

As follows from the TG data (curve *2* in Fig. 3b), in the temperature range of 530–750 K, the $Sr_{2.4}Dy_{0.6}Co_2O_{5.90}$ sample is oxidized and the formal Co^{n+} oxidation state n increases from $n = 2.6$ ($T = 300$ K, $\Delta m = 3.30\%$) to $n = 3.5$ ($T = 750$ K, $\Delta m = 2.87\%$), which was calculated using the data from Fig. 3b (curve *1*). The formal average oxidation state of cobalt is $n = 3$ (Co^{3+}) at $T = 700$ K. A value of $n = 2.6$ at $T = 300$ K is in quantitative agreement with the number $N_2$of Co^{2+}–Co^{2+} dimers. A value of $n < 3$ at $T < 700$ K shows that, along with Co^{3+} ions, the system contains Co^{2+} ions, the concentration of which decreases with increasing temperature due to oxidation of the sample. At $T \approx 700$ K, we have $n = 3$, but this state is unstable and some Co^{3+} ions disproportionate to Co^{2+} and Co^{4+} ions. With an increase in temperature, the Co^{4+} ion concentration increases and, at $T > 700$, we have $n > 3$ K.

Taking into account a fairly high temperature of the observed anomalies and the thermal analysis data (Fig. 3), to explain the sharp drop of the Seebeck coefficient and the change in its sign, let us consider the charge disproportionation $2Co^{3+} \leftrightarrow Co^{2+} + Co^{4+}$ [36] at $T \approx 700$ K.

Using the generalized Heike's formula for the thermopower of cobalt oxides [37].

$$S_H = -\frac{k_B}{e}\ln\left(\frac{g_3}{g_2}\frac{1-x_2}{x_2}\right) \quad (8)$$

where k_B is the Boltzmann constant; g_2 and g_3 are the degeneracies of Co^{2+} and Co^{3+} ions, respectively; and x_2 is the Co^{2+} ion concentration, we can present the Seebeck coefficient at $T < T_C \approx 700$ K in the form$S = S_r + S_H$, whereS_r is the regular component unrelated to the orbital and spin multiplicity of cobalt ions. At $T \approx 700$ K, the x_2 value tends to zero and the S_H value logarithmically diverges in the negative region. At high temperatures ($T > T_C$), the system contains a certain amount of Co^{2+}, Co^{4+} and Co^{3+} ions; therefore, the Heike component S_H cannot be presented in simple form (8).

4. Conclusions

A new anion-deficient $Sr_{2.4}Dy_{0.6}Co_2O_{7-\delta}$ ($\delta = 1.1$–0.33) perovskite phase with a structure of the second term of the $A_3B_2O_7$ Raddlesden–Popper homologous series was synthesized. The obtained phase has a tetragonal unit cell with sp. gr. *I4/mmm*. The data of the thermal analysis showed that the compositions of both the "reduced" $Sr_{2.4}Dy_{0.6}Co_2O_{5.9}$ and "oxidized" $Sr_{2.4}Dy_{0.6}Co_2O_{6.67}$ RP phases are invariable at $T < 530$ K in an inert or oxidizing atmosphere. At higher temperatures, the $Sr_{2.4}Dy_{0.6}Co_2O_{7-\delta}$ phase can reversibly absorb/release oxygen. The magnetic properties of the synthesized samples were studied in the temperature range of 10–400 K and described in terms of formation of dimers, in which the Co^{3+}–Co^{3+} and Co^{2+}–Co^{2+} ionic pairs antiferromagnetically interact and are in the nonmagnetic ground state. The electrical conductivity and Seebeck coefficient were measured in air at temperatures from 300 to 800 K. A sharp decrease in the Seebeck coefficient of the $Sr_{2.4}Dy_{0.6}Co_2O_{6.09}$ phase and the change in its sign near 700 K were attributed to the transition of cobalt ions to the Co^{3+} state and the charge disproportionation of Co^{3+} ions to Co^{2+} and Co^{4+} ones.

Although the Seebeck coefficient S at room temperature is fairly high, the electrical conductivity has low values. This leads to the low thermoelectric power factor $P(T)$ (Fig. 5d), which does not allow one to consider this compound as a thermoelectric material. However, taking into account the redox processes occurring in the investigated sample, such compounds can be considered as potential resistive switches for memristive devices [38] or anode materials for supercapacitors when the anion charge storage through oxygen intercalation was proposed [39].

Declaration of competing interest

The authors declare that they have no known competing financial interests or personal relationships that could have appeared to influence the work reported in this paper.

Acknowledgments

The study was supported by the Russian Foundation for Basic Research, project no. 19-03-00017 and the budget project #AAAA-A17-117021310222-4 for the Institute of Chemistry and Chemical Technology, Siberian Branch of the Russian Academy of Sciences.

References

[1] S.N. Ruddlesden, P. Popper, The compound $Sr_3Ti_20_7$ and its structure, Acta Cryst 11 (1958) 54–55, https://doi.org/10.1107/S0365110X58000128.
[2] S.N. Ruddlesden, P. Popper, New compounds of the K_2NiF_4 type, Acta Cryst 10 (1957) 538–539, https://doi.org/10.1107/S0365110X57001929.
[3] B.V. Beznosikov, K.S. Aleksandrov, Perovskite-like crystals of the Ruddlesden-Popper series, Crystallogr. Reports 45 (2000) 792–798, https://doi.org/10.1134/1.1312923.
[4] A. Demont, S. He'bert, D. Pelloquin, A. Maignan, The $Sr_{2.75}Ce_{0.25}Co_2O_{7-\delta}$ oxide, $n = 2$ member of the Ruddlesden–Popper series: structural and magnetic evolution depending on oxygen stoichiometry, Journal of Solid State Chemistry 181 (2008) 1314–1320, https://doi.org/10.1016/j.jssc.2008.02.023.
[5] E. Naumovich, M. Patrakeev, V. Kharton, A. Yaremchenko, D. Logvinovich, F. Marques, Oxygen nonstoichiometry in $La_2Ni(M)O_{4+\delta}$ (M = Cu, Co) under oxidizing conditions, Solid State Sciences 7 (2005) 1353–1362, https://doi.org/10.1016/j.solidstatesciences.2005.08.005.
[6] J.G. Bednorz, K.A. Mueller, Possible high T_c superconductivity in the Ba−La−Cu−O system, Phys. B: Condens. Matter 64 (1986) 189–193, https://doi.org/10.1007/BF01303701.
[7] R.J. Cava, R.B. van Dover, B. Batlogg, E.A. Rietman, Bulk superconductivity at 36 K in $La_{1.8}Sr_{0.2}CuO_4$, Phys. Rev. Lett. 58 (1987) 408, https://doi.org/10.1103/PhysRevLett.58.408.
[8] Y. Moritomo, A. Asamitsu, H. Kuwahara, Y. Tokura, Giant magnetoresistance of manganese oxides with a layered perovskite structure, Nature London 380 (1996) 141–144, https://doi.org/10.1038/380141a0.
[9] K. Yamaura, D.P. Young, R.J. Cava, Thermally induced variable-range-hopping crossover and ferromagnetism in the layered cobalt oxide $Sr_2Y_{0.5}Ca_{0.5}Co_2O_7$, Phys. Rev. B 63 (2001), 064401, https://doi.org/10.1103/PhysRevB.63.064401.
[10] K. Yamaura, Q. Huang, R.J. Cava, Synthesis, crystal structure, electrical, and magnetic properties of the new layered cobalt oxides (Sr, Ca, Ln)$_3Co_2O_{6\pm\delta}$ (ln = Sm, Eu, Gd, Tb, Dy, Ho, and Y), Journal of Solid State Chemistry 146 (1999) 277–286, https://doi.org/10.1006/jssc.1999.8375.
[11] T.F. Sheshko, T.A. Kryuchkova, YuM. Serov, I.V. Chislova, I.A. Zvereva, New mixed perovskite-type $Gd_{2-x}Sr_{1+x}Fe_2O_7$ catalysts for dry reforming of methane, and production of light olefins, Catal. Ind. 9 (2017) 162–169, https://doi.org/10.1134/S207050417020009X.
[12] K.-W. Song, K.-T. Lee, Characterization of $NdSrCo_{1-x}Fe_xO_{4+\delta}$ ($0 \le x \le 1.0$) intergrowth oxide cathode materials for intermediate temperature solid oxide fuel cells, Ceramics International 37 (2011) 573–577, https://doi.org/10.1016/j.ceramint.2010.10.004.
[13] J. Zhou, G. Chen, K. Wu, Y. Cheng, J. Power Sources 1232 (2013) 332–337.
[14] Z. Zhang, H. Wu, X. Meng, J. Li, Z. Zhan, Evaluation of $GdSrCoO_{4+\delta}$ inter growth oxides as cathode materials for intermediate-temperature solid oxide fuel cells, Electrochimica Acta 133 (2014) 509–514, https://doi.org/10.1016/j.electacta.2014.04.078.
[15] G. Mazo, N. Lyskov, L. Leonova, Morphology and electrochemical characterization of $LaSrCuO_{4-\delta}|Ce_{0.9}Gd_{0.1}O_{2-\delta}$ interface, Solid State Ionics 182 (2011) 64–70, https://doi.org/10.1016/j.ssi.2010.11.011.
[16] J. Wan, J. Goodenough, J. Zhu, $Nd_{2-x}La_xNiO_{4+\delta}$, a mixed ionic/electronic conductor with interstitial oxygen, as a cathode material, Solid State Ionics 178 (2007) 281–286, https://doi.org/10.1016/j.ssi.2007.01.013.
[17] B. Peng, G. Chen, T. Wang, J. Zhou, J. Guo, Y. Cheng, K. Wu, Hydride reduced $LaSrCoO_{4-\delta}$ as new cathode material for $Ba(Zr_{0.1}Ce_{0.7}Y_{0.2})O_3$ based intermediate temperature solid oxide fuel cells, Journal of Power Sources 201 (2012) 174–178, https://doi.org/10.1016/j.jpowsour.2011.10.121.
[18] A.J. Jacobson, Materials for solid oxide fuel cells, Chem. Mater. 22 (2010) 660–674, https://doi.org/10.1021/cm902640j.
[19] K. Koumoto, I. Terasaki, R. Funahashi, Complex oxide materials for potential thermoelectric applications, MRS BULLETIN 31 (2006) 206–210, https://doi.org/10.1557/mrs2006.46.

[20] K. Koumoto, Y. Wang, R. Zhang, A. Kosuga, R. Funahashi, Oxide thermoelectric materials: a nanostructuring approach, Annu. Rev. Mater. Res. 40 (2010) 363–394, https://doi.org/10.1146/annurev-matsci-070909-104521.
[21] T.I. Chupakhina, N.V. Melnikova, O.I. Gyrdasova, YuA. Nikitina, V. G. Gavrilyachenko, YuV. Kabirov, H.B. Прущакова, E.V. Chebanova, E.B. Rusakova, Inženernyj vestnik Dona (Rus) 4 (2016).
[22] N.B. Ivanova, S.G. Ovchinnikov, M.M. Korshunov, I.M. Eremin, N.V. Kazak, The features of spin, charge and orbital orderings in the cobaltites, Phys. Usp. 52 (2009) 789–810, https://doi.org/10.3367/UFNr.0179.200908b.0837.
[23] A. Ahad, D.K. Shukla, F. Rahman, S. Majid, Tarachand, G.S. Okram, A.K. Sinha, D. M. Phase, Colossal thermopower, spin states and delocalization effects in single layered $La_{2-x}Sr_xCoO_4$, Acta Materialia 135 (2017) 233–243, https://doi.org/10.1016/j.actamat.2017.06.030.
[24] S.N. Vereshchagin, V.A. Dudnikov, N.N. Shishkina, L.A. Solovyov, Phase transformation behavior of $Sr_{0.8}Gd_{0.2}CoO_{3-\delta}$ perovskite in the vicinity of order-disorder transition, Thermochimica Acta 655 (2017) 34–41, https://doi.org/10.1016/j.tca.2017.06.003.
[25] L.J. Gillie, J. Hadermann, M. Hervieu, A. Maignan, C. Martin, Oxygen vacancy ordering in the double-layered ruddlesden-popper cobaltite $Sm_2BaCo_2O_{7-\delta}$, Chem. Mater 20 (2008) 6231–6237, https://doi.org/10.1021/cm8010138.
[26] L.A. Solovyov, Full-profile refinement by derivative difference minimization, Journal of Applied Crystallography 37 (2004) 743–749, https://doi.org/10.1107/S0021889805004899.
[27] K. Conder, E. Pomjakushina, A. Soldatov, E. Mitberg, Oxygen content determination in perovskite-type cobaltates, Materials research bulletin 40 (2005) 257–263, https://doi.org/10.1016/j.materresbull.2004.10.009.
[28] A.T. Burkov, A.I. Fedotov, A.A. Kasyanov, R.I. Panteleev, T. Nakama, Methods and technique of thermopower and electrical conductivity measurements of thermoelectric materials at high temperatures, Scientific and Technical Journal of Information Technologie 15 (2015) 173–195, https://doi.org/10.17586/2226-1494-2015-15-2-173-195.
[29] L. Viciu, H.W. Zandbergen, Q. Xu, Q. Huang, M. Lee, R.J. Cava, J. Solid State Chem 179 (2006) 500–511, https://doi.org/10.1016/j.jssc.2005.11.013.
[30] L.J. Gillie, A.J. Wright, J. Hadermann, G. Van Tendeloo, C. Greaves, Synthesis and characterization of the reduced double-layer manganite $Sr_3Mn_2O_{6+x}$, J. Solid State Chem. 175 (2003) 188–196, https://doi.org/10.1016/S0022-4596(03)00245-7.
[31] N. Nguyen, L. Er-Rakho, C. Michel, J. Choisnet, B. Raveau, Intercroissance de feuillets "perovskites lacunaires" et de feuillets type chlorure de sodium: les oxydes $La_{2-x}A_{1+x}Cu_2O_{6-x}/2$ (A = Ca, Sr), Mater. Res. Bull. 15 (1980) 891–897, https://doi.org/10.1016/0025-5408(80)90212-3.
[32] A.K. Zvezdin, V.M. Matveev, A.A. Mukhin, A.I. Popov, Rare Earth Ions in Magnetically Ordered Crystals, Izdatel'stvo Nauka, Moscow, 1985 (In Russian).
[33] Z. Hu, Hua Wu, M.W. Haverkort, H.H. Hsieh, H.-J. Lin, T. Lorenz, J. Baier, A. Reic Tanakahl, I. Bonn, C. Felser, A. Tanaka, C.T. chen, L.H. Tjeng, Different look at the spin state of Co^{3+} ions in a CoO_5 pyramidal coordination, Phys. Rev. Lett. 92 (2004) 207402, https://doi.org/10.1103/PhysRevLett.92.207402.
[34] C. He, H. Zheng, J.F. Mitchell, M.L. Foo, R.J. Cava, C. Leighton, Low temperature Schottky anomalies in the specific heat of $LaCoO_3$: defect-stabilized finite spin states, Appl. Phys. Lett. 94 (2009) 102514, https://doi.org/10.1063/1.3098374.
[35] T.N. Vasil'chikova, T.G. Kuz'mova, A.A. Kamenev, A.R. Kaul, A.N. Vasil'ev, Spin states of cobalt and the thermodynamics of $Sm_{1-x}Ca_xCoO_{3-\delta}$ solid solutions, JETP Lett 97 (2013) 34–37, https://doi.org/10.7868/S0370274X13010074.
[36] C. Autret, J. Hejtmanek, K. Knızek, M. Marysko, Z. Jirak, M. Dlouha, S. Vratislav, Electric transport and magnetic properties of perovskites $LaMn_{1-x}Co_xO_3$ up to 900 K, J. Phys.: Condens. Matter 17 (2005) 1601–1616, https://doi.org/10.1088/0953-8984/17/10/015.
[37] W. Koshibae, K. Tsutsui, S. Maekawa, Thermopower in cobalt oxides, Phys. Rev. B 62 (2000) 6869–6872, https://doi.org/10.1103/PhysRevB.62.6869.
[38] V.R. Nallagatla, T. Heisig, C. Baeumer, V. Feyer, M. Jugovac, G. Zamborlini, C. M. Schneider, R. Waser, M. Kim, C.U. Jung, R. Dittmann, Topotactic phase transition driving memristive behavior, Adv. Mater. 31 (2019) 1903391, https://doi.org/10.1002/adma.201903391.
[39] Hao-shan Nan, Xiao-ying Hu, Hong-wei Tian, Recent advances in perovskite oxides for anion-intercalation supercapacitor: a review, Materials Science in Semiconductor Processing 94 (2019) 35–50, https://doi.org/10.1016/j.mssp.2019.01.033.